

# 1 Improvement of the KarstMod modeling 2 platform for a better assessment of karst 3 groundwater resources

4 Vianney Sivellev<sup>1</sup>, Guillaume Cinkus<sup>1,2</sup>, Naomi Mazzilli<sup>2</sup>, David Labat<sup>3</sup>, Bruno Arfib<sup>4</sup>, Nicolas Massei<sup>5</sup>,  
5 Yohann Cousquer<sup>1</sup>, Dominique Bertin<sup>6</sup> and Hervé Jourde<sup>1</sup>

6  
7 <sup>1</sup> HSM, Univ Montpellier, CNRS, IRD, Montpellier, France

8 <sup>2</sup> EMMAH, INRAE, Avignon Université, 84000 Avignon, France

9 <sup>3</sup> Géosciences Environnement Toulouse UMR CNRS IRD Université Paul Sabatier CNES, 14 Avenue  
10 Edouard Belin 31400, Toulouse

11 <sup>4</sup> Aix-Marseille Univ, CNRS, IRD, INRAE, Coll de France, CEREGE, Aix-en-Provence, France

12 <sup>5</sup> Univ Rouen Normandie, Univ Caen Normandie, CNRS, M2C, UMR 6143, F-76000 Rouen, France

13 <sup>6</sup> GEONOSIS, France

14 Correspondence: vianney.sivelle@umontpellier.fr

## 15 **Abstract**

16 Hydrological models are fundamental tools for the characterization and management of karst systems.  
17 We propose an updated version of KarstMod, software dedicated to lumped parameter rainfall-discharge  
18 modeling of karst aquifers. KarstMod provides a modular, user-friendly modeling environment for  
19 educational, research, and operational purposes. It also includes numerical tools for time series analysis,  
20 model evaluation, and sensitivity analysis. The modularity of the platform facilitates common operations  
21 related to lumped parameter rainfall-discharge modeling, such as (i) setup and parameter estimation of  
22 a relevant model structure, and (ii) evaluation of internal consistency, parameter sensitivity, and  
23 hydrograph characteristics. The updated version now includes (i) external routines to better consider the  
24 input data and their related uncertainties, i.e. evapotranspiration and solid precipitation, (ii) enlargement  
25 of multi-objective calibration possibilities, allowing more flexibility in terms of objective functions as  
26 well as observation type and (iii) additional tools for model performance evaluation including further  
27 performance criteria and tools for model errors representation.

## 28 **1 Introduction**

29 Karst aquifers constitute an essential source of drinking water for about 9.2% of the world population  
30 (Stevanović, 2019) and it is estimated that one-quarter of the world population depends on freshwater  
31 from karst aquifers (Ford and Williams, 2013). Karst aquifers contain an important volume of freshwater

32 while only 1% of its annually renewable water is used for drinking water supply (Stevanović, 2019).  
33 Understanding the functioning of karst aquifers and developing operational tools to predict the evolution  
34 of freshwater resources is therefore a major challenge for the hydrological science community (Blöschl  
35 et al., 2019). To this day, the number of tools dedicated to karst hydrogeology is limited and is mostly  
36 developed for academic purposes and not user-friendly. Nonetheless, such tools are required for a better  
37 assessment of groundwater vulnerability as well as sustainable management of the groundwater  
38 resources (Elshall et al., 2020) and should be handled by the stakeholders without programming skills  
39 requirements.

40 KarstMod is an adjustable modeling platform (Mazzilli et al., 2019) dedicated to lumped parameter  
41 rainfall-discharge modeling allowing for (i) simulation of spring discharge, piezometric head and  
42 surface water discharge (Bailly-Comte et al., 2010; Cousquer and Jourde, 2022; Sophocleous, 2002),  
43 (ii) analysis of the internal fluxes considered in the model, (iii) model performance evaluation and  
44 parametric sensitivity analysis. In this paper, we present the new features incorporated in KarstMod: (i)  
45 external routines to better consider the input data and their related uncertainties, i.e. evapotranspiration  
46 and solid precipitation, (ii) enlargement of multi-objective calibration possibilities, allowing more  
47 flexibility in terms of objective functions as well as observation type with the possibility to include  
48 surface water discharge in the calibration procedure and (iii) model performance evaluation, including  
49 additional performance criteria as well as additional tools for model errors representation such as the  
50 diagnostic efficiency plot (Schwemmler et al., 2021). Also, we present two case studies to illustrate how  
51 KarstMod is useful in the framework of the assessment of karst groundwater resources and its sensitivity  
52 to groundwater abstraction. Section 2 is devoted to the presentation of the background and motivations  
53 to improve the functionalities of the platform while Sect. 3 presents the key features of KarstMod.  
54 Section 4 illustrates the application of rainfall-discharge modeling using KarstMod within the Touvre  
55 (western France) and the Lez (southern France) karst systems, which both constitute strategic freshwater  
56 resources and ensure drinking water supply.

## 57 **2 Background and motivations**

### 58 **2.1 Challenges in karst groundwater resources**

59 Karst aquifers are affected by the combination of different components of global change such as (i)  
60 effects of climate change which are particularly pronounced in the Mediterranean area (Dubois et al.,  
61 2020; Nerantzaki and Nikolaidis, 2020), (ii) increasing groundwater abstraction (Labat et al., 2022), as  
62 well as (iii) changes in land cover land use (Bittner et al., 2018; Sarrazin et al., 2018). Therefore, the  
63 assessment of karst groundwater resources sensitivity, in terms of quantity, requires operational tools  
64 for estimating the sustainable yield of karst aquifers but also to predict the impacts of climatic or  
65 anthropogenic forcing on groundwater resources in the long term (Sivelle et al., 2021). To address these  
66 issues, different modeling approaches have been developed (Jeannin et al., 2021) such as, among others,

67 fully-distributed models (Chen and Goldscheider, 2014), semi-distributed models (Doummar et al.,  
68 2012; Dubois et al., 2020; Ollivier et al., 2020), and lumped parameter models (Mazzilli et al., 2019)  
69 including semi-distributed recharge (Bittner et al., 2018; Sivelles et al., 2022b). Among these, lumped  
70 parameter models are recognized as major tools to explore the ability of conceptual representations to  
71 explain observations in karst systems (Duran et al., 2020; Frank et al., 2021; Poulain et al., 2018; Sivelles  
72 et al., 2019) and for managing karst groundwater resources (Cousquer and Jourde, 2022; Labat et al.,  
73 2022; Sivelles et al., 2021; Sivelles and Jourde, 2020).

## 74 **2.2 Challenges in lumped parameters modeling in karst hydrology**

75 Lumped parameter models consist of a functional approach that analyzes a hydrogeological system at  
76 the catchment scale and describes the transformation from rainfall into discharge using empirical or  
77 conceptual relationships. Therefore, parameter values or distributions cannot be determined directly  
78 from catchment physical characteristics or in-situ measurements, except the discharge coefficient to the  
79 spring that can be estimated based on recession curve analysis. Instead, model parameter values must  
80 be estimated by history-matching. In a general way, rainfall-discharge models in karst hydrology are  
81 calibrated considering spring discharge measurements. Former studies have shown an interest in  
82 considering hydrochemical observations (Chang et al., 2021; Hartmann et al., 2013; Sivelles et al., 2022a)  
83 but such an approach requires further methodological development before being included in KarstMod.  
84 To date, KarstMod allows considering complementary observations only with piezometric head and  
85 surface water discharge (Cousquer and Jourde, 2022).

86 Another challenge concerns the evaluation of the water fluxes within the soil-vegetation-atmosphere  
87 continuum. Bittner et al. (2021) computed several models to evaluate the fluxes related to interception,  
88 evapotranspiration, and snow process. The results show significant uncertainties related to input data as  
89 well as potential compensation between the various uncertain processes. In some cases, snow melt is a  
90 controlling factor in the water balance (Doummar et al., 2018; Liu et al., 2021), thus a suitable snowmelt  
91 estimation is required to improve hydrological model performance (Çallı et al., 2022). Therefore, two  
92 meteorological modules have been added to KarstMod: (i) a "Snow routine" and (ii) a routine to compute  
93 the potential evapotranspiration  $PET$  ( $\text{mm day}^{-1}$ ), denoted "PET routine". The two additional modules  
94 allow us to better account for snow and evapotranspiration processes.

## 95 **3 Implementation**

96 The updated version of KarstMod implements additional features to enhance the rainfall-discharge  
97 modeling practices. First, we describe the additional modules (snow and PET routines) for a better  
98 meteorological forcing estimation. Then, we introduce the additional tools proposed for (i) the setup and  
99 calibration of the model structure, (ii) model performance evaluation as well as (iii) uncertainties  
100 consideration. Fig. 1 shows a screenshot of the KarstMod software.

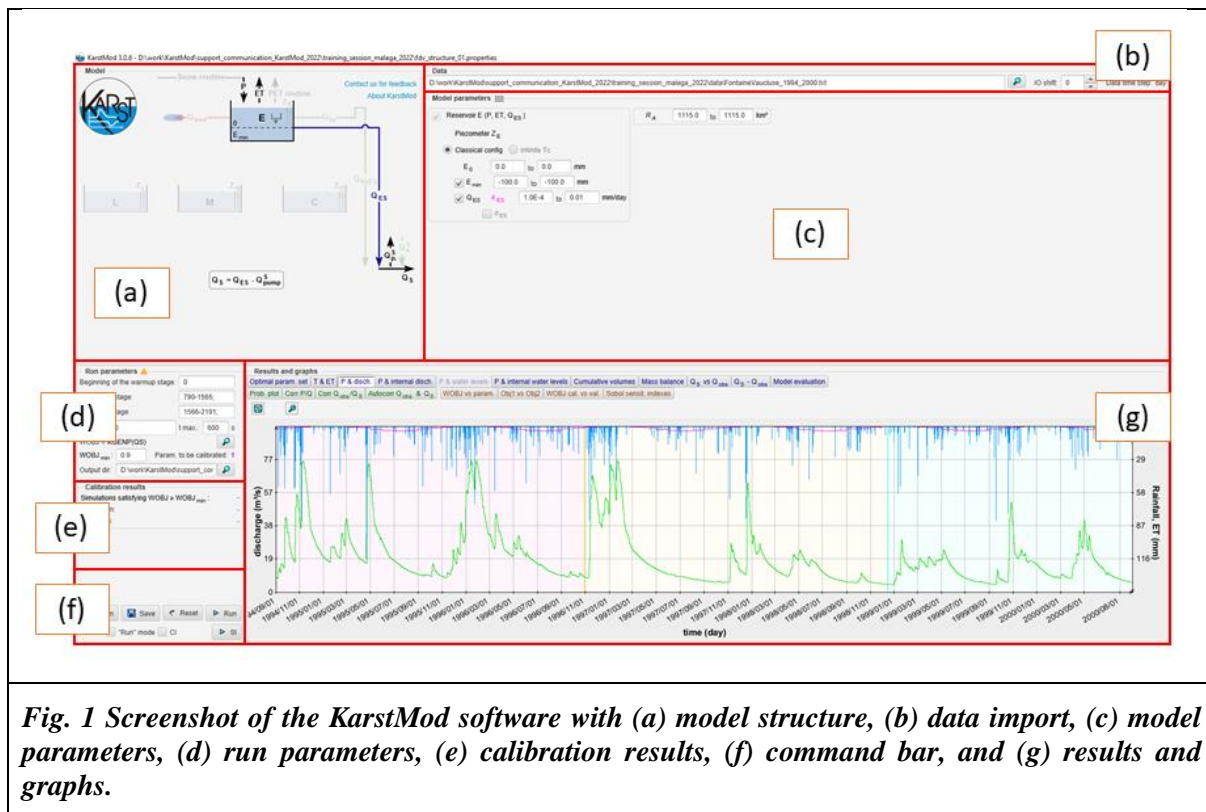


**Fig. 1** Screenshot of the KarstMod software with (a) model structure, (b) data import, (c) model parameters, (d) run parameters, (e) calibration results, (f) command bar, and (g) results and graphs.

### 101 3.1 Meteorological modules

#### 102 3.1.1 Snow routine

103 KarstMod allows using either observation-based precipitation time series  $P$  (mm day<sup>-1</sup>) or estimated  
 104 precipitation time series  $P_{Sr}$  (mm day<sup>-1</sup>) using a snow routine. The latter is similar to the one used by  
 105 Chen et al. (2018) – without the radiation components – which has been successfully used for improving  
 106 the simulation of karst spring discharge in snow-covered karst systems (Chen et al., 2018; Cinkus et al.,  
 107 2023a). It consists of a modified HBV-snow routine (Bergström, 1992) for simulating snow  
 108 accumulation and melt over different sub-catchments based on altitude ranges. Each sub-catchment is  
 109 defined by two values that the user must input: (i) the proportion among the whole catchment (sum must  
 110 be equal to 1) and (ii) the temperature shift, related to the altitude gradient. The different estimated  
 111 precipitation  $P_{Sr}^*$  (mm day<sup>-1</sup>) associated with the subcatchments are calculated and summed to produce  
 112 the estimated precipitation time series  $P_{Sr}$ , which corresponds to a single variable representative of the  
 113 catchment.  $P_{Sr}$  thus gives the water leaving the snow routine and is equivalent to the recharge into the  
 114 first compartment of the model (compartment E in KarstMod). The snow routine workflow requires  
 115 both air temperature  $T$  (°C) and precipitation  $P$  (mm day<sup>-1</sup>) time series.  $P$  is considered as snow when  $T$   
 116 in the sub-catchment is lower than the temperature threshold  $T_s$  (°C). Snow melts when the temperature  
 117 exceeds the threshold according to a degree-day expression. The snow melt is a function of the melt  
 118 coefficient  $MF$  (mm °C<sup>-1</sup> day<sup>-1</sup>), and the degrees above the temperature threshold. Runoff starts when  
 119 the water level exceeds the liquid water holding capacity of snow  $CWH$  (-). The refreezing coefficient

120 *CFR* (-) stands for refreezing liquid water in the snow when snow melt is interrupted (Bergström, 1992).  
 121 The output of the snow routine consists of a redistributed precipitation time series  $P_{sr}$ . The four  
 122 parameters of the snow routine (i.e.,  $T_s$ ,  $MF$ ,  $CWH$ , and  $CFR$ ) can be considered in the parameter  
 123 estimation procedure as well as sensitivity analysis. The snow routine features can be activated from the  
 124 model structure area (Fig. 1 a). Fig. 2 shows the general workflow implemented in the snow routine.  $P_{sr}^*$   
 125 is estimated for each time step  $t$  based on the precipitation  $P$  and air temperature  $T$  time series for each  
 126 sub-catchment  $i$ . The total snow routine output  $P_{sr}$  is calculated as a weighted sum of  $P_{sr}^*$  time series:

$P_{sr} = \sum_i^N P_{sr_i}^* \times p_i$	<b>Eq. 1</b>
---	--------------

127 where  $p_i$  is the proportion of the sub-catchment  $i$  regarding the complete catchment area such as  $\sum p_i =$   
 128 1, and  $N$  is total number of sub-catchments. The snow routine allows estimating  $P_{sr}^*$  according to the  
 129 algorithm A1.

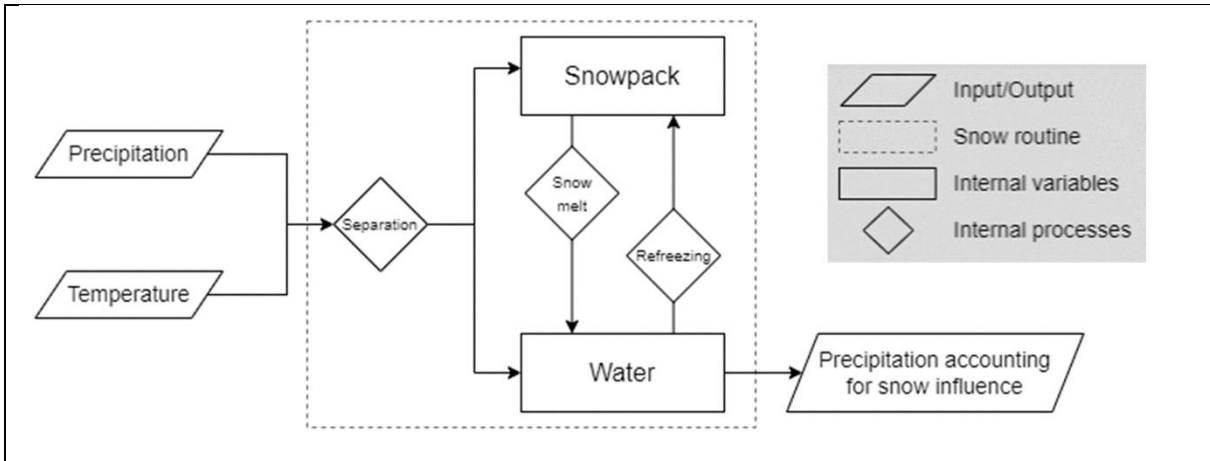


**Fig. 2 Snow routine workflow.**

130

---

**Algorithm A1** Estimating  $P_{sr}^*$  in sub-catchment

---

With  $P_{sr}^*$  = water leaving the routine/recharge to the soil ( $\text{mm day}^{-1}$ ),  $T_a$  = active temperature for snowmelt ( $^{\circ}\text{C}$ ),  $T_n$  = active temperature for refreezing ( $^{\circ}\text{C}$ ),  $m$  = snow melt ( $\text{mm day}^{-1}$ ),  $rfz$  = refreezing ( $\text{mm day}^{-1}$ ),  $v$  = solid component of snowpack depth (mm),  $vl$  = liquid component of snowpack depth (mm), and  $dt$  = temporal resolution.

**for  $t$  in time do :**

```

| m[t] = min(MF × Ta [t], v[t]) with Ta [t] = T[t] - Ts
| rfz[t] = min(CFR × MF × Tn [t], vl[t]) with Tn [t] = Ts - T[t]
| v[t+dt] = v[t] - m[t] + snow[t] + rfz[t]
| if vl[t+dt] > CWH × v[t+dt] then

```

```

    |   |  $P_{Sr}^* [t] = vl[t+dt] - CWH \times v[t+dt]$ 
    |   |  $vl[t+dt] = CWH \times v[t+dt]$ 
    |   |
    |   | else
    |   |   |  $P_{Sr}^* [t] = 0$ 
    |   |   |
    |   | end
end

```

---

### 131 3.1.2 Potential Evapotranspiration routine

132 An additional module allows to compute the potential evapotranspiration  $PET$  (mm day<sup>-1</sup>) based on the  
 133 Oudin’s formula (Oudin et al., 2005). The  $PET$  routine can be activated from the model structure area  
 134 (Fig. 1 a). The  $PET$  routine affects only compartment E. The latter stands for soil and epikarst storage  
 135 zone, where the water is available for actual evapotranspiration  $AET$  (mm day<sup>-1</sup>) and flows toward  
 136 infiltration or surface discharge. Infiltration occurs when the water level in the compartment is greater  
 137 than a given threshold  $E_{min}$ , otherwise, the compartment is considered under-saturated and does not  
 138 produce infiltration. In this case, the water in compartment E is still available for evapotranspiration.  
 139 KarstMod allows us to consider evapotranspiration in four separate ways (Fig. 3):

140 (a) The water transfer in the soil-atmosphere continuum can be pre-processed by the user. In this case,  
 141 the given precipitation time series consists of the effective precipitation  $P_{eff}$  (mm day<sup>-1</sup>), derived  
 142 from precipitation  $P$  (mm day<sup>-1</sup>) and actual evapotranspiration  $AET$  (mm day<sup>-1</sup>) with Eq. 2. The  
 143 evapotranspiration flux is not activated in the model structure selection panel in KarstMod (Fig. 1  
 144 a).

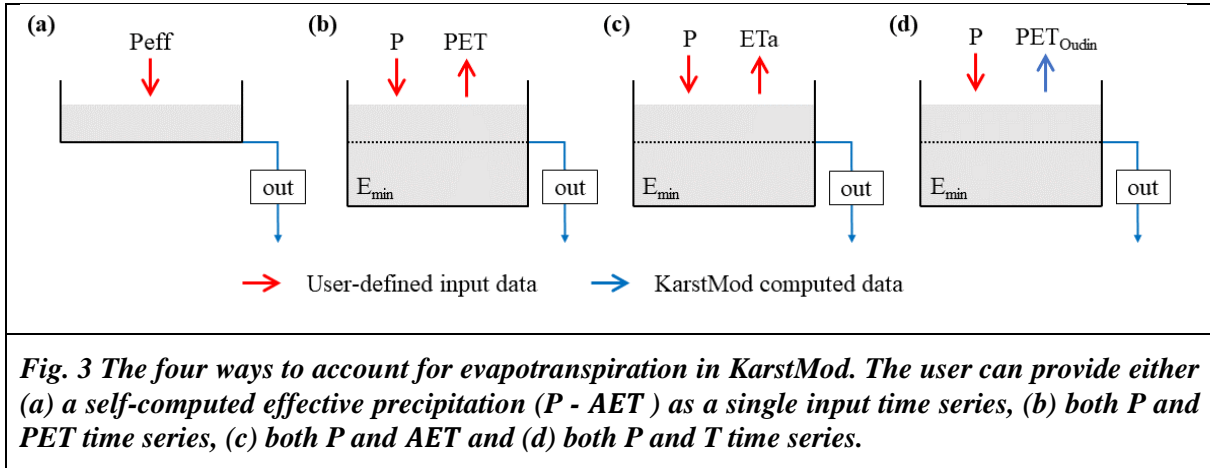
$P_{eff} = P - AET$	<b>Eq. 2</b>
---------------------	--------------

145 (b) User-defined  $PET$  can be given as input in KarstMod for the evapotranspiration time series. Using  
 146  $E_{min}$ , the user can simulate water holding capacity and non-linear behavior of karst recharge.  
 147 (c) User-defined  $AET$  can be given as input data in KarstMod for evapotranspiration time series instead  
 148 of  $PET$ . Then, KarstMod computes an estimation of effective precipitation by limiting the  
 149 evapotranspiration to water content available in compartment E. The simulated  $AET$  can then be  
 150 lower than the user defined  $AET$ . Such configuration may help identifying potential inaccuracy of  
 151 user defined  $AET$  for the modeling purpose but is not recommended for model set-up and parameter  
 152 estimation.  
 153 (d) The new feature in KarstMod consists of the  $PET$  routine which estimates the  $PET$  with the Oudin’s  
 154 formula (Oudin et al., 2005) (Eq. 3). It needs a  $T$  time series and two parameters to be estimated,  
 155 which can be considered in the parameter estimation procedure as well as sensitivity analysis.

$$PET = \left( \frac{R_e}{\lambda \times \rho} \right) \times \left( \frac{T + K2}{K1} \right) \text{ if } T + K2 > 0 \text{ else } PET = 0$$

**Eq. 3**

156 where  $R_e$  is the extraterrestrial radiation ( $\text{MJ m}^{-2} \text{ day}^{-1}$ ) depending only on the latitude and the Julian  
 157 day,  $\lambda$  is the latent heat flux (taken equal to  $2.45 \text{ MJ kg}^{-1}$ ),  $\rho$  is the density of water (taken equal to  $1000$   
 158  $\text{kg m}^{-3}$ ) and  $T$  is the mean daily air temperature ( $^{\circ}\text{C}$ ).  $K1$  ( $^{\circ}\text{C}$ ) and  $K2$  ( $^{\circ}\text{C}$ ) are constants to adjust over  
 159 the catchment for rainfall-discharge model (Oudin et al., 2005). In KarstMod, both  $K1$  and  $K2$  can be  
 160 considered in the parameter estimation procedure as well as sensitivity analysis.



### 161 3.2 Set-up and calibration of the model structure

162 The modular structure proposed in KarstMod is based on a widely used conceptual model which  
 163 separates karst aquifers into an infiltration zone and a saturated zone, or low and quick flows through  
 164 the unsaturated and saturated zones (Fleury et al., 2007, 2009; Guinot et al., 2015; Mazzilli et al., 2019;  
 165 Sivellev et al., 2019). Based on this conceptual representation, the platform offers four compartments  
 166 organized as a two-level structure: (i) compartment E (higher level) and (ii) compartments L, M and C  
 167 (lower level). A priori, the higher level represents the infiltration zone or the soil and epikarst. At the  
 168 lower level, compartments L, M, and C stand for the different sub-systems of the saturated zone or low  
 169 and quick flows of the whole hydro system. The various model structures and their governing equations  
 170 are presented in Mazzilli et al. (2022; 2019). Also, KarstMod allows to performance of hydrological  
 171 modeling on both daily and hourly temporal resolutions (Sivellev et al., 2019).

172 The user can activate (or deactivate) the various compartments (E, L, M, and C) within the "model  
 173 structure" panel (Fig. 1 a). The solid and faded colors represent the activated and the inactivated features,  
 174 respectively. The fluxes and their activation thresholds as well as the exponent of the discharge law  $\alpha$   
 175 (in case of non-linear discharge law such  $\alpha \neq 1$ ) are managed from the "model parameters" panel (Fig.  
 176 1 c). The user can account for pumping  $Q_{pump}$  (water coming out of the compartment) as well as sinking  
 177 stream  $Q_{sink}$  (water coming into the compartment). Such an option is available only if the user provides  
 178 the required time series (Fig. 1 b).

179 The user must provide warm-up, calibration, and validation periods (Fig. 1 d). The warm-up period must  
 180 be set to be independent of initial conditions to avoid bias in the parameter estimation procedure  
 181 (Mazzilli et al., 2012). Then, a calibration period (i.e. the period in which the parameters are estimated  
 182 to reduce the predictive errors) and a validation period (i.e. period separated from the calibration period)  
 183 can be defined to run the split sample test procedure (Klemeš, 1986). For calibration purpose, KarstMod  
 184 proposes several widely used performance criteria  $\phi$ : the Pearson's correlation coefficient  $R_p$   
 185 (Freedman et al., 2007), the Spearman rank correlation coefficient  $R_s$  (Freedman et al., 2007), the Nash-  
 186 Sutcliffe Efficiency NSE (Nash and Sutcliffe, 1970), the volumetric error VE (Criss and Winston, 2008),  
 187 the modified balance error BE (Perrin et al., 2001), the Kling-Gupta Efficiency KGE (Gupta et al., 2009)  
 188 and a non-parametric variant of the Kling-Gupta Efficiency KGENP (Pool et al., 2018). To compute a  
 189 multi-objective calibration procedure the user can create his objective function  $\Phi$  as a weighted sum of  
 190 several objective functions:

$\Phi = \sum_{i=1}^N \omega_i \times \phi_i(U)$	<b>Eq. 4</b>
---	--------------

191 where  $\omega_i$  is the weight affected to the objective function  $\phi_i(U)$  with  $\sum_{i=1}^N \omega_i = 1$  and  $U$  a general  
 192 notation for the observations used for parameter estimation purposes. In the KarstMod modeling  
 193 platform,  $U$  corresponds to either spring discharge  $Q_s$ , piezometric head measurements  $Z_{obs}$  (available  
 194 for compartments E, L, M, and C), or surface water discharge  $Q_{loss}$  from compartment E. Also, the  
 195 objective function  $\phi$  can be computed on transformed  $U$  to avoid high water level bias on quadratic  
 196 error. The following transformations are available in KarstMod:  $1/U$ ,  $\sqrt{U}$ ,  $1/\sqrt{U}$ . Therefore, the user  
 197 can use any combination of the objective function  $\phi$ , observations  $U$ , and variable transformations.  
 198 Depending on the modeling purpose, the user must refer to the literature to define the suitable objective  
 199 function (Bennett et al., 2013; Ferreira et al., 2020; Hauduc et al., 2015; Jackson et al., 2019).

200 The model is calibrated using a quasi-Monte-Carlo sampling procedure with a Sobol sequence sampling  
 201 of the parameter space (Sobol, 1998). The procedure involves finding an ensemble of parameter sets  
 202 providing an objective function  $\Phi$  greater than the user-defined value. The calibration procedure  
 203 stopped when either the user-defined maximum duration of the sampling procedure  $t_{max}$  is reached or  
 204 the user-defined number of parameter sets  $n_{obj}$  are collected. KarstMod offers a "run" option allowing  
 205 the model to run for a user-defined parameter set, without calibration procedure, and so allows it to  
 206 investigate "by-hand" the parameter space and the sensitivity of the model to specific parameters.

### 207 **3.3 Model evaluation**

208 The model performance can be evaluated for both the calibration and validation periods. It allows (i) to  
 209 ensure the robustness of model predictions, even under changing conditions (which is a key point for  
 210 the assessment of climate change impact) and (ii) to avoid model over-fitting within a specific range of



211 hydro-climatic conditions observed during the calibration period. KarstMod allows the computation of  
212 the above-mentioned performance criteria for both calibration and validation periods. Even though the  
213 notation "validation" is disputable such a procedure is required to evaluate both explanatory and  
214 predictive dimensions of the model structure (Andréassian, 2023). Then, KarstMod offers an ensemble  
215 of numerical tools devoted to (i) checking the model consistency, i.e. explanatory dimension of the  
216 model (Beven, 2001; Shmueli, 2010), (ii) evaluating the model performance, i.e. predictive dimension  
217 of the model structure.

218 To check the model consistency, the simulation based on the parameter set that provides the highest  
219 objective function value can be analyzed through an ensemble of graphs such as (i) internal and external  
220 fluxes as a function of time, (ii) cumulative volumes for both observed and simulated time series for  
221 spring discharge  $Q_s$  and surface water discharge  $Q_{loss}$ , (iii) simulated mass-balance as a function of  
222 time, (iv) comparison of observations and simulations for either  $Q_s$  or  $Q_{loss}$  with probability function  
223 plots, auto-correlogram of the spring discharge time series, cross-correlogram of precipitation-discharge  
224 time series.

225 To evaluate the model performance, KarstMod offers a "Model evaluation" panel available from the  
226 graphs panel (Fig. 1 g) that includes several sub-panels, from the left to the right:

- 227 • The diagnostic efficiency DE (Schwemmler et al., 2021) which consists of a diagnostic polar plot  
228 that facilitates the model evaluation process as well as the comparison of multiple simulations. The  
229 DE accounts for constant, dynamics, and timing errors, and their relative contribution to the model  
230 errors. Also, the decomposition of the errors between the periods of high flows and low flows allows  
231 us to better investigate the model bias, as well as to provide critical evaluation for impact studies,  
232 particularly for the assessment of climate change impacts. Indeed, the accurate evaluation of low  
233 flow periods (in terms of frequency, intensity, and duration) becomes increasingly crucial for  
234 groundwater resource variability assessment.
- 235 • The available objective functions  $\Phi$  are presented as a radar chart which consists of a polygon where  
236 the position of each point from the center gives the value of the performance criteria. The closer the  
237 point is to the outside of the radar chart, the better the model performs. The radar chart is made for  
238 both calibration and validation periods and each of the calibration variables considered in the  
239 modeling ( $Q_s$ ,  $Z_{obsA}$  with A for either E, M, C or L compartments and  $Q_{loss}$ ).
- 240 • The KGE (Gupta et al., 2009) consists of a diagonal decomposition of the NSE (Nash and Sutcliffe,  
241 1970) to separate Pearson's correlation coefficient  $R_p$ , representation of bias  $\beta_{KGE}$ , and variability  
242  $\alpha_{KGE}$ . Thus, the  $KGE$  is comparable to multi-objective criteria for calibration purposes  
243 (Pechlivanidis et al., 2013). The sub-panel offers (i) a bi-plot of the three  $KGE$ 's components and  
244 (ii) a radar plot visualization of the  $KGE$ 's components, allowing the identify potential  
245 counterbalancing errors according to these different components (Cinkus et al., 2023b). The two

246 above-mentioned plots also include the decomposition of the *KGENP* (Pool et al., 2018) in terms of  
247 Spearman's rank correlation coefficient  $R_s$ , representation of bias  $\beta_{KGENP}$  and non-parametric  
248 variability  $\alpha_{KGENP}$ .

### 249 **3.4 Dealing with uncertainties**

250 Moges et al. (2021) summarize the various sources of uncertainties in hydrological models including  
251 structural and parametric uncertainties as well as uncertainties related to input data and observations.  
252 The latter concerns both the input (i.e., precipitation and evapotranspiration) and the output (i.e.,  
253 discharge) of the modeled systems. Many references are devoted to the uncertainties related to input  
254 data and observations. As an example, Westerberg et al. (2020) include information about the discharge  
255 uncertainty distribution in the objective function and perform better discharge simulation. Also, the  
256 precipitation error can be dependent on the data time step (McMillan et al., 2011) and could impact the  
257 hydrological model performance (Ficchi et al., 2016). Lumped parameter hydrological models consider  
258 meteorological time series representative of a whole catchment, which may require some pre-processing,  
259 particularly for snow processes since it can have a strong influence on flow dynamics. Thus, KarstMod  
260 includes variables related to both the snow routine (i.e., the redistributed precipitation time series  $P_{sr}$ )  
261 and the PET routine (i.e., estimated potential evapotranspiration  $PET$ ) in the parameter estimation  
262 procedure. This allows us to investigate the sensitivity of the flow simulation to these input data when  
263 using snow and PET routines. Nonetheless, KarstMod does not include features to investigate the impact  
264 of observation uncertainties on parameter estimation.

265 As with many environmental problems, parameter estimation in rainfall-discharge modeling consists  
266 generally of ill-posed problems, i.e. the modeling encounters issues about the unicity, identifiability, and  
267 stability of the problem solution (Ebel and Loague, 2006). As a consequence, several representations of  
268 the modeled catchment may be considered equally acceptable (Beven, 2006). Knoben et al. (2020)  
269 evaluate the performance of 36 daily lumped parameter models over 559 catchments and show that  
270 between 1 and up to 28 models can show performance close to the model structure with the highest  
271 performance criteria. Such results are widely covered in catchment hydrology (Dakhlaoui and Djebbi,  
272 2021; Darbandsari and Coulibaly, 2020; Gupta and Govindaraju, 2019; Pandi et al., 2021; Zhou et al.,  
273 2021) but still poorly investigated in karst hydrology. Indeed, the structural uncertainty impacts on  
274 rainfall-discharge modeling in karst hydrology is not properly evaluated whereas many studies consider  
275 several hydrological model structures to include structural uncertainty in flow simulation (Hartmann et  
276 al., 2012; Jiang et al., 2007; Jones et al., 2006; Sivelles et al., 2021). KarstMod includes more than fifty  
277 combinations of the various compartments as well as various compartments model (i.e., compartment  
278 with linear or non-linear discharge law and compartment with infinite characteristic time) and allows a  
279 quick implementation of the various model structures. The user can easily manage to start the modeling  
280 with one single compartment and gradually move to a more complex model structure with up to four

281 compartments, five fluxes connected to the spring, four internal fluxes, and 1 flux running out of the  
282 system.

283 Considering each model structure, parametric equifinality can be investigated using (i) dot plots of the  
284 values of the objective function against the parameter values, (ii) dot plots of the values of the  
285 performance criteria used to define the aggregated objective function, and (iii) the variance-based, first-  
286 order  $S_i$  and total  $ST_i$  sensitivity indexes for the model parameters. Details concerning the computation  
287 of sensitivity indexes within KarstMod are given in Mazzilli et al. (2022; 2019).

## 288 **4 Examples of application**

289 To illustrate the KarstMod application and the use of the above-presented functionalities for the  
290 assessment of karst groundwater resources, we propose two case studies: (i) the Touvre karst system  
291 and (ii) the Lez karst system. Both karst systems consist of strategic freshwater resources for drinking  
292 water supply (DWS), for the city of Angoulême (western France) and Montpellier (southern France)  
293 respectively.

### 294 **4.1 The Touvre karst system (La Rochefoucauld)**

295 The Touvre is a karst system where the infiltration consists of (i) a delayed infiltration of effective  
296 precipitation on the karstic recharge area and (ii) a direct infiltration of surface water from the Tardoire,  
297 Bandiat, and Bonnieure rivers. The latter are surface streams flowing on metamorphic rocks that partly  
298 infiltrate to subterranean at the contact with carbonate formations, mainly composed of Middle to Upper  
299 Jurassic limestones. The springs of the Touvre, located 7 km east of Angoulême (western France), counts  
300 four outlets, namely the Bouillant, the Dormant, the Font de Lussac, and the Lèche (Labat et al., 2022).  
301 In the following, the Touvre Spring discharge designates the accumulated discharge of the four  
302 mentioned outlets.

303 The Touvre karst system constitutes a strategic freshwater resource for the DWS of Angoulême, with  
304 around 110,000 inhabitants, but also contributes to the water supply for industry and agriculture. In  
305 2015, there were eighty-four pumping wells over the karstic impluvium of the Touvre karst system, and  
306 around one hundred more in the Tardoire, Bandiat, and Bonnieure rivers catchment. Based on the data  
307 provided by the Adour-Garonne Water Agency, the annual groundwater abstraction for agriculture  
308 represents  $4.6 \text{ Mm}^3$  whereas annual groundwater abstraction for DWS represents  $1.1 \text{ Mm}^3$  over the  
309 karstic impluvium of the Touvre karst system. On the three rivers catchment (out of the karstic  
310 impluvium), the annual groundwater abstraction represents  $2.5 \text{ Mm}^3$  for agriculture and  $3.3 \text{ Mm}^3$  for  
311 DWS, through river intakes or alluvial groundwater abstraction. The total annual volume of abstracted  
312 groundwater in the area represents around 5 % of the annual volume of transit at the Touvre Spring.  
313 This is quite low compared with karst aquifers in France exploited for their groundwater resources, such  
314 as the Lez spring (Jourde et al., 2014) and the Oeillal's spring karst catchment (Sivelle et al., 2021),  
315 where the annual groundwater abstraction volume represents respectively 50 % and 15 % of the annual

316 volume of transit at the spring. Therefore, the Touvre karst system seems not to be over-exploited at the  
317 moment, but the impact of groundwater abstraction should be addressed in the context of global change  
318 to ensure sustainable management of this strategic freshwater resource.

319 The area is characterized by an ocean-influenced climate with a mean annual precipitation of around  
320 800 mm year<sup>-1</sup> distributed over an average of 255 rainy days. The estimation is performed with Thiessen  
321 polygon methods based on eleven meteorological stations over the area (Labat et al., 2022). The mean  
322 annual potential evapotranspiration is around 770 mm year<sup>-1</sup> according to the Penman-Monteith  
323 estimation provided by the French meteorological survey (Météo-France). The Touvre daily spring  
324 discharge shows a significant variability ranging from 3 m<sup>3</sup> s<sup>-1</sup> to 49 m<sup>3</sup> s<sup>-1</sup> with a coefficient of variation  
325 around 0.46 (Fig. 5 b).

326 The surface stream flow rates for the Bonnieure, Bandiat, and Tardoire rivers are concentrated within  
327 the autumn and winter periods. During the summer period, the discharge in the three rivers is very low  
328 (Fig. 5 c). The more significant groundwater abstraction is performed during the summer period, while  
329 the Touvre spring discharge reaches its lowest values within the late summer and early autumn periods  
330 (Fig. 5, c and d).

331 Fig. 4 shows the model structure for the Touvre karst system that consists of three compartments  
332 organized in two levels (Labat et al., 2022). The upper level corresponds to reservoir E and represents  
333 both the unsaturated part of the system and a temporary aquifer. This reservoir relates to the two  
334 reservoirs of the lower level: C (Conduit) and M (Matrix) representative of quick and slow flow  
335 dynamics, respectively. The upper level of the model structure is affected by  $P$  and  $ET$  while the lower  
336 level of the model structure is affected by (i) groundwater abstraction and (ii) sinking river streamflow  
337 from the surface to underground. Fig. 4 shows the various time series required for the hydrological  
338 modeling of the Touvre karst system. The methodology for daily time series preparation given in Labat  
339 et al. (2022) allows us to account for the influence of groundwater abstraction on the transmissive or  
340 capacitive part of the karst aquifer as well as the influence of concentrated and diffuse infiltration of the  
341 surface river streamflow.

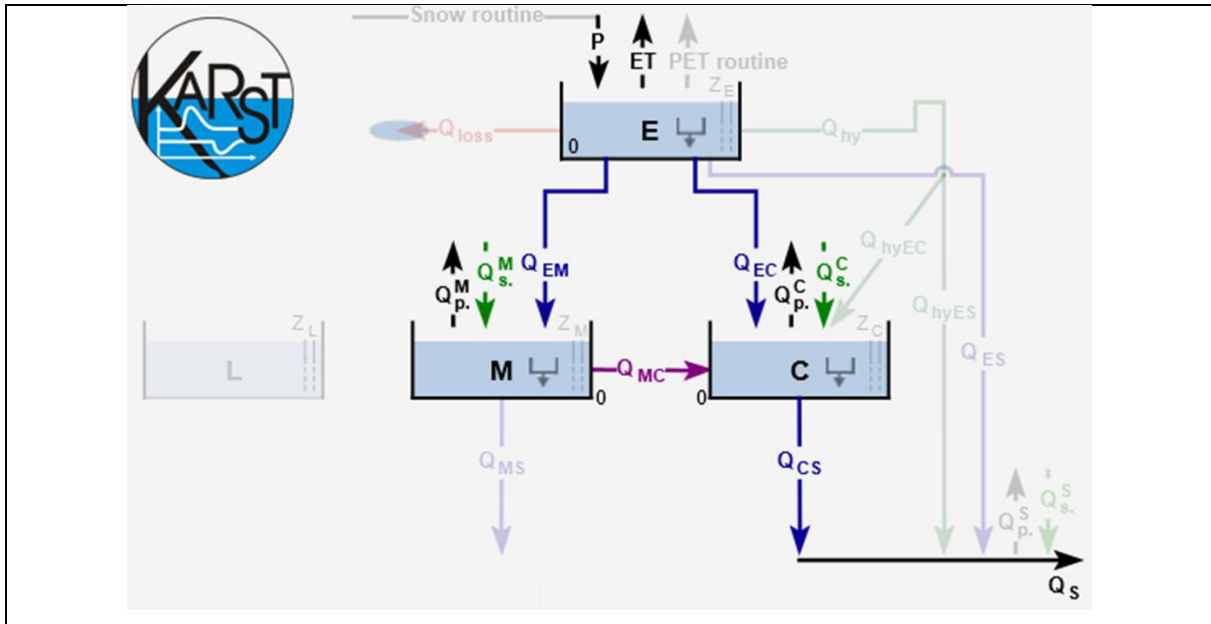


**Fig. 4** Screenshot of KarstMod with a focus on the panel "Model structure" for the Touvre karst system. The solid lines correspond to the activated fluxes whereas the faded color lines are not activated.  $Q_p^M$  and  $Q_p^C$  stand for groundwater abstraction that affects compartments M and C respectively while  $Q_s^M$  and  $Q_s^C$  stand for sinking flow that affects compartments M and C, respectively.

342

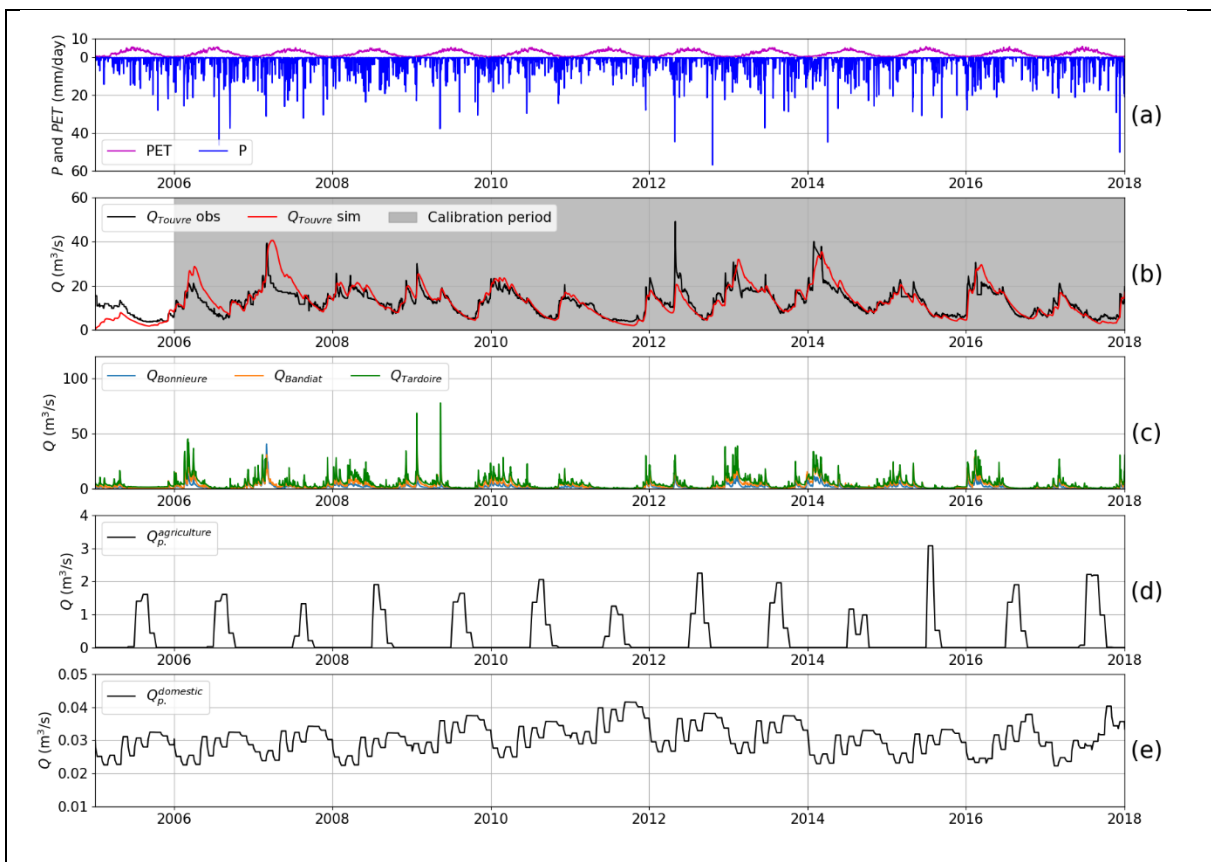


**Fig. 5** Daily time series for the Touvre system: a) precipitation (P) and potential evapotranspiration (PET), b) observed and simulated karst spring discharge ( $Q_{Touvre\ obs}$  and  $Q_{Touvre\ sim}$ ), c)

*observed river streamflow discharge ( $Q_{Bonnieur}$ ,  $Q_{Bandiat}$ ,  $Q_{Tardoire}$ ),  $d$ ) and  $e$ ) groundwater abstraction discharge ( $Q_{agriculture}^{agg}$ ,  $Q_{p}^{dom}$ ).*

343 The objective of the hydrological modeling is to assess the impact of groundwater abstraction on spring  
 344 discharge, more particularly during low flow periods (Labat et al., 2022). So, the calibration is performed  
 345 according to the *KGENP* that improves the simulations during mean and low-flow conditions using the  
 346 Spearman rank correlation due to its insensitivity to extreme values (Pool et al., 2018). The sampling  
 347 procedure is set up to find  $n_{obj} = 5000$  simulations with *KGENP* greater than 0.9. Afterwards, the model  
 348 is evaluated using the various features proposed in KarstMod (Fig. 6). The diagnostic efficiency plot  
 349 (Fig. 6 a) testifies of several elements: (i) the model seems to slightly overestimate high flow and  
 350 underestimate low flow, (ii) the timing error is about 0.9, testifying of suitable flow dynamics in the  
 351 model, (iii) low flow periods contribute more to the model errors, and (iv) there is no offset in the  
 352 simulated spring hydrograph. The radar chart (Fig. 6 b) shows a good equilibrium between the various  
 353 objective functions whose values are greater than 0.8, except for the NSE criteria (NSE = 0.75). It is the  
 354 consequence of the design of these criteria that tends to outweigh the errors during floods. Here the NSE  
 355 value is still greater than 0.7 and testifies to a "very good" fit according to Moriasi et al. (2007). Finally,  
 356 the decomposition of the KGE (Fig. 6 c and d) shows  $R_p = 0.91$ ,  $\alpha = 1.15$  and  $\beta = 1.02$  testifying of  
 357 accurate dynamics and low bias, but slightly too high variability.

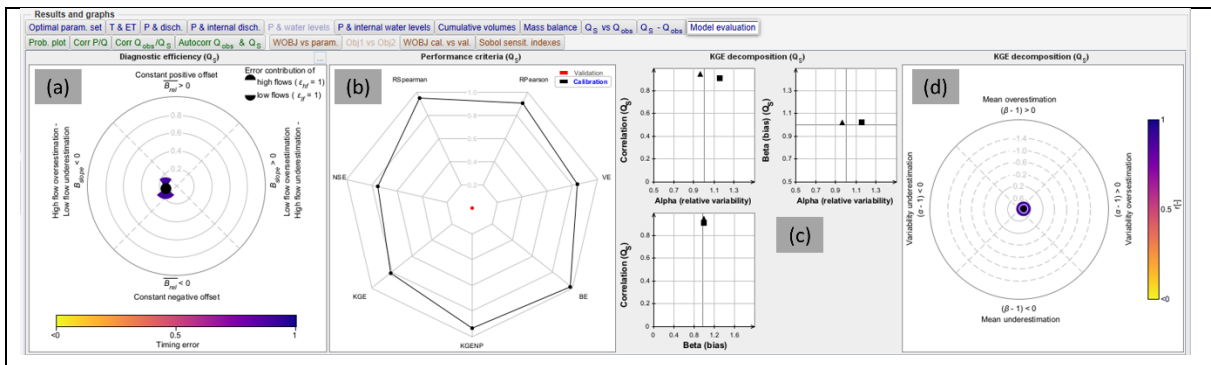


**Fig. 6 Screenshot of KarstMod with a focus on the sub-panel "Model evaluation". Application for the model evaluation on the Touvre system: (a) diagnostic efficiency plot (Schwemmler et al., 2021), (b) radar chart of the objective functions, (c) bi-plot of the KGE's (square) and KGENP's (triangle) components, and (d) radar chart of the KGE's components.**

## 358 4.2 The Lez Spring

359 The Lez Spring (southern France) consists of the main outlet of a karst system encompassed in the North  
 360 Montpellieran Garrigue hydrogeological unit delimited to the west by the Herault River, and to the north  
 361 and east by the Vidourle River. The geology in the area corresponds to the Upper Jurassic layers  
 362 separated by the Corconne-Matelle fault (oriented N30°), leading to two main compartments in the  
 363 aquifer (Bérard, 1983; Clauzon et al., 2020). The karst aquifer is unconfined in the western compartment  
 364 and is locally confined in the eastern compartment. The Lez Spring is located about 15 km north of  
 365 Montpellier. It is of Vauclusian-type with an overflow level at 65 m a.s.l and a maximum daily discharge

366 of approximately  $15 \text{ m}^3 \text{ s}^{-1}$ . The area is characterized by a typical Mediterranean climate with dry  
367 summers and rainy autumns. Over the 2009-2019 period, the mean annual precipitation is around 900  
368  $\text{mm year}^{-1}$  distributed over an average of 133 rainy days (estimation with Thiessen polygon methods  
369 based on four meteorological stations over the area: Prades-le-Lez, Saint-Martin-de-Londres,  
370 Sauteyrargues, and Valflaunès), a mean annual potential evapotranspiration is around  $900 \text{ mm year}^{-1}$   
371 according to the estimation based on Oudin's formula with the temperature measured at Prades le Lez  
372 station while the real annual evapotranspiration is around  $450 \text{ mm year}^{-1}$  (eddy covariance flux-station  
373 of Puéchabon).

374 Since 1854, the Lez Spring supplies the drinking water to Montpellier city and the surroundings. It  
375 currently constitutes the main freshwater resource for around 350,000 people in the area. The present  
376 water management scheme allows pumping at higher rates than the natural spring discharge during low  
377 flow periods, while supplying a minimum discharge rate (around  $0.23 \text{ m}^3 \text{ s}^{-1}$ ) into the Lez River to ensure  
378 ecological flow downstream, and reducing flood hazards via rainfall storage in autumn (Avias, 1995;  
379 Jourde et al., 2014). The pumping plant was built in 1982 with four deep wells drilled to intercept the  
380 karst conduit feeding the spring, 48 m below the overflow level of the spring. Pumping in these wells  
381 allows up to  $0.18 \text{ m}^3 \text{ s}^{-1}$  to be withdrawn under low flow periods (with an authorized maximum  
382 drawdown of 30 m), while the average annual pumping flow rate is about  $0.10 \text{ m}^3 \text{ s}^{-1}$  (over the 2008-  
383 2019 period). Due to the pumping management of the aquifer, which supplies about 30 to 35  $\text{Mm}^3$  of  
384 water per year to the metropolitan area of Montpellier, the discharge at the Lez Spring is often low or  
385 nil. Discharge is also measured downstream (Lavalette gauging station) where the measured discharge  
386 corresponds to the Lez Spring discharge and the main tributaries (Lirou and Terrieu streams) which flow  
387 essentially after intense Mediterranean rainfall events. As suggested in Cousquer and Jourde (2022), the  
388 surface water discharge, denoted  $Q_{loss}$ , can be estimated as the difference between the total discharge  
389 in Lavalette and the Lez spring discharge.

390 In the present context of global change, Mediterranean karst systems already show significant decrease  
391 in spring discharge (Doummar et al., 2018; Dubois et al., 2020; Fiorillo et al., 2021; Hartmann et al.,  
392 2012; Nerantzaki and Nikolaidis, 2020; Smiatek et al., 2013) which could be aggravated with  
393 groundwater abstraction (Sivelle et al., 2021). The Lez spring is strongly exposed to global change  
394 impact: (i) the Mediterranean area is identified as a climate change hot-spot (Diffenbaugh and Giorgi,  
395 2012) where the projected warming spans  $1.8\text{--}8.4^\circ\text{C}$  according to CMIP6 and  $1.2\text{--}6.6^\circ\text{C}$  according to  
396 CMIP5 during the summer period (Cos et al., 2022), and (ii) the water management scheme will have  
397 to adapt to the future need in drinking water for the growing population in the area as well as changes  
398 in the freshwater consumption practice (e.g. water use restriction order). Therefore, a sustainable water  
399 management plan for the Lez Spring requires a good appreciation of the hydrological functioning as  
400 well as the operational hydrological model to properly address impact studies. In this framework,  
401 KarstMod allows for choosing and calibrating a suitable model structure. This constitutes the first step

402 for a global change impact study that requires prediction tools to simulate the aquifer response to various  
 403 external forces.

404 Fig. 7 shows the model structure for the Lez karst catchment (Mazzilli et al., 2011) that consists of three  
 405 compartments organized in two levels. The upper level corresponds to compartment E and represents  
 406 the unsaturated part of the system, including a soil water holding capacity  $E_{min}$  and a discharge lost  
 407 from the compartment  $Q_{loss}$ . Compartment E is exposed to  $P$  and  $ET$  and discharge towards the lower  
 408 level of the model structure starts when the water level exceeds  $E_{min}$ . The lower level consists of two  
 409 inter-connected compartments M and C allowing to reproduction of the lateral exchanges, denoted  $Q_{MC}$ .  
 410 between the transmissive function (compartment C) and the capacitive function (compartment M) of the  
 411 karst aquifer. Both M and C compartments are considered bottomless, allowing to reproduce periods of  
 412 non-overflow at the Lez Spring when the mean water level in the aquifer stands below 65 m a.s.l., mainly  
 413 during summer periods due to pumping in the karst conduit. Fig. 8 a and b show the various daily time  
 414 series required for the hydrological modeling of the Lez karst system (i.e.,  $P$ ,  $ET$  and  $Q_{pump}$ ).

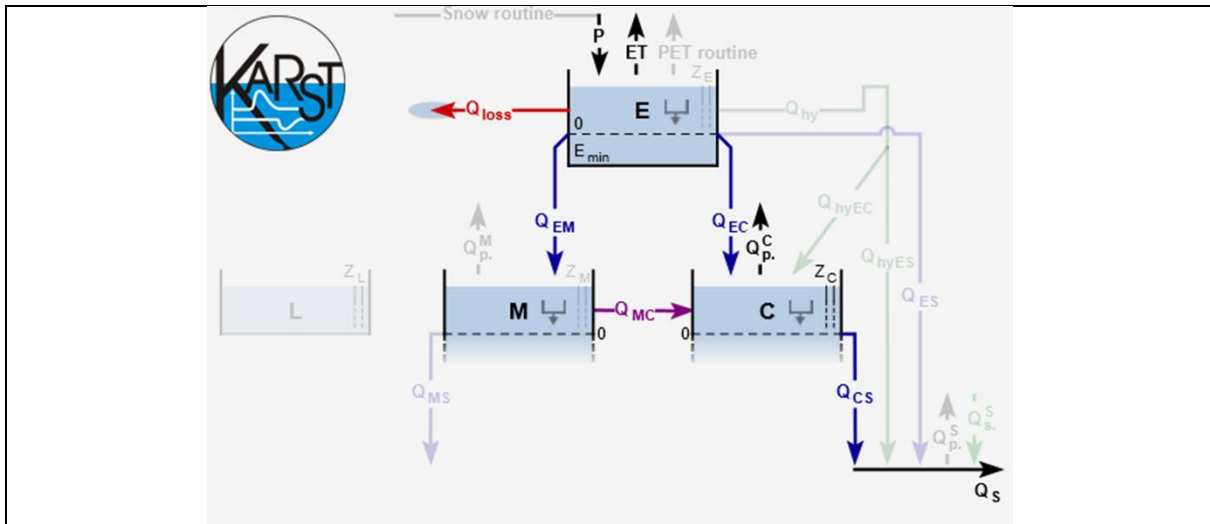


**Fig. 7 Screenshot of KarstMod with a focus on the panel "Model structure" for the Lez karst system. The solid lines correspond to the activated fluxes whereas the faded color lines are not activated.  $Q_{loss}$  stands for the surface water discharge from the epikarst compartment,  $Q_{p}^C$  stands for groundwater abstraction that affects compartments C while  $Z_C$  stands for piezometric head measurements considered as representative of compartment C.**

415



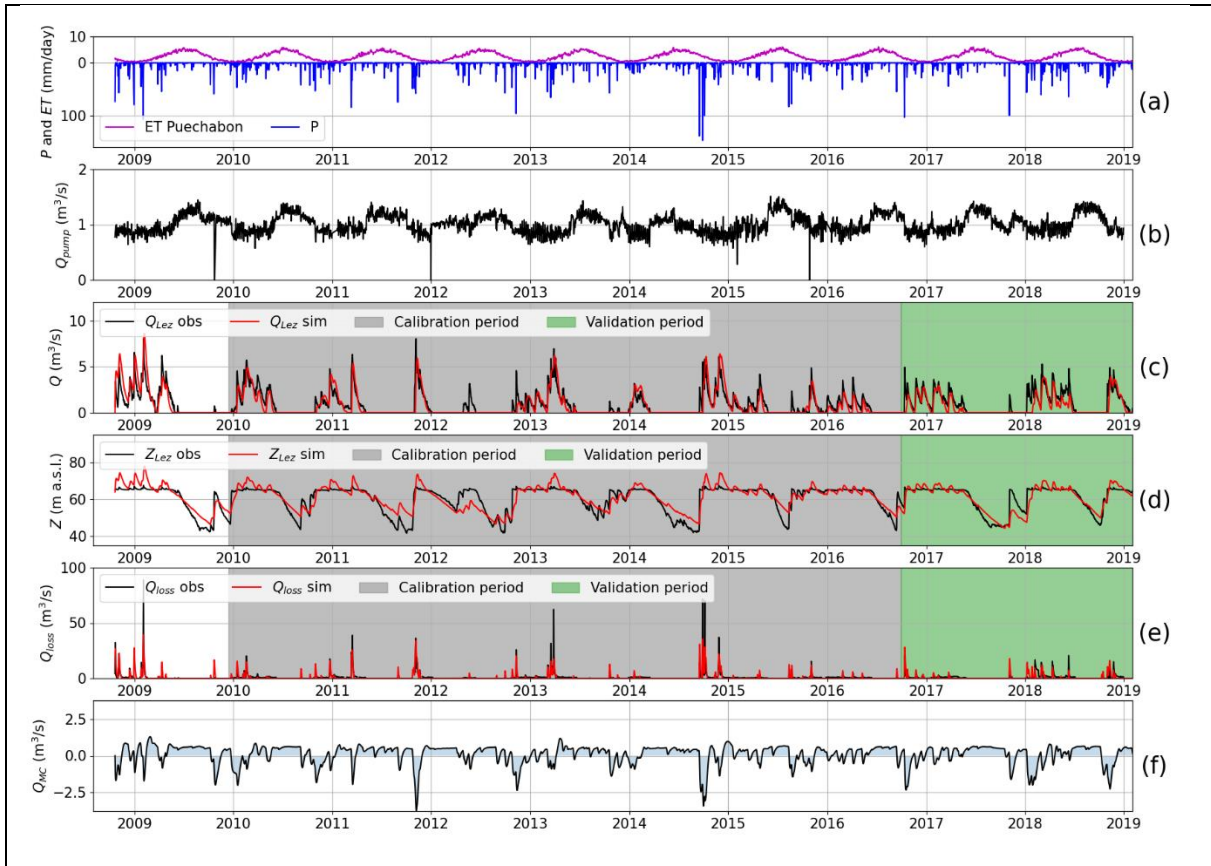


**Fig. 8 Daily time series for the Lez system: a) precipitations ( $P$ ) and evapotranspiration ( $ET$ ), b) groundwater abstraction,  $Q_{pump}$ , c) observed and simulated karst spring discharge ( $Q_{Lez\ obs}$  and  $Q_{Lez\ sim}$ ), d) observed and simulated piezometric head ( $Z_{Lez\ obs}$  and  $Z_{Lez\ sim}$ ), e) surface water discharge ( $Q_{loss}$ ) and f) simulated exchanges fluxes between compartment M and C,  $Q_{MC}$ .**

416 The available hydrological observations for model calibration consist of spring discharge  $Q_S$ ,  
 417 piezometric head measurement  $Z_C$  at the Lez spring, and surface water discharge from secondary outlets  
 418 and intermittent springs  $Q_{loss}$  (Fig. 8 c, d, and e).

419 The surface water discharge is estimated as the difference in discharge measured at the Lavalette station  
 420 (15 km downstream of the Lez spring) and the discharge measured at the Lez spring, as proposed by  
 421 Cousquer and Jourde (2022). Therefore,  $Q_{loss}$  includes all the water loss from the epikarst within several  
 422 seasonal overflowing springs (i.e., Lirou spring, Restinclière spring, and Fleurette spring). KarstMod  
 423 allows for easy handling of the various parameter estimations depending on the considered hydrological  
 424 observations (i.e., spring discharge, piezometric head measurement, and surface discharge from the  
 425 epikarst). The sampling procedure is set up to find  $n_{obj} = 5000$  simulations with an aggregated objective  
 426 function  $\Phi$  greater than 0.6. As suggested by Cousquer and Jourde (2022), using complementary  
 427 hydrological observations in addition to the spring discharge allows for to reduce the parametric  
 428 uncertainties in the modeling of the Lez spring discharge. Therefore, using a multi-objective calibration  
 429 procedure implemented in KarstMod, the objective function is built such as:

$$\Phi = \frac{1}{3} \times NSE(Q_s) + \frac{1}{3} \times NSE(Z_c) + \frac{1}{3} \times NSE(Q_{loss})$$

Eq. 5

430 The calibration procedure leads to an optimal  $\Phi = 0.65$  decomposed such as  $\phi Q_s = 0.70$ ,  $\phi Z_c = 0.57$   
 431 and  $\phi Q_{loss} = 0.70$  within the calibration period. Model performance evaluation on the validation period  
 432 shows suitable model performance for both spring discharge and piezometric with  $\phi Q_s = 0.54$  and  $\phi Z_c$   
 433  $= 0.79$ , but poor model performance according to the surface water discharge with  $\phi Q_{loss} = 0.36$ .  
 434 Afterwards, the results can be evaluated using the various features proposed in KarstMod (Fig. 9). The  
 435 results show higher model performances for  $Q_s$  and  $Z_c$  than for  $Q_{loss}$ . The model performance appears  
 436 quite satisfactory concerning the variable of interest to assess the impact of the water management  
 437 scheme on the groundwater resources within the Lez aquifer.

438 The simulated exchange fluxes between compartments M and C (Fig. 8 f) show consistent dynamics  
 439 with the observations. Indeed, during periods of high flow, the exchange fluxes are oriented from  
 440 compartment C to compartment M (i.e.,  $Q_{MC} < 0$ ). Significant precipitation events lead to rapid rises in  
 441 the piezometric head, saturation of the transmissive part of the aquifer, and finally the establishment of  
 442 overflow at the Lez spring (i.e.  $Q_s > 0$ ) as well as the overflowing springs (i.e.  $Q_{loss} > 0$ ). Conversely,  
 443 during the periods of low piezometric head (i.e., both  $Q_s$  and  $Q_{loss}$  are nil), the simulated exchange  
 444 fluxes are oriented from compartment M to compartment C (i.e.  $Q_{MC} > 0$ ). Such flow exchanges between  
 445 capacitive and transmissive parts of karst aquifers have been evidenced using KarstMod on other karst  
 446 environment (Duran et al., 2020; Frank et al., 2021; Labat et al., 2022; Sivelles et al., 2019).

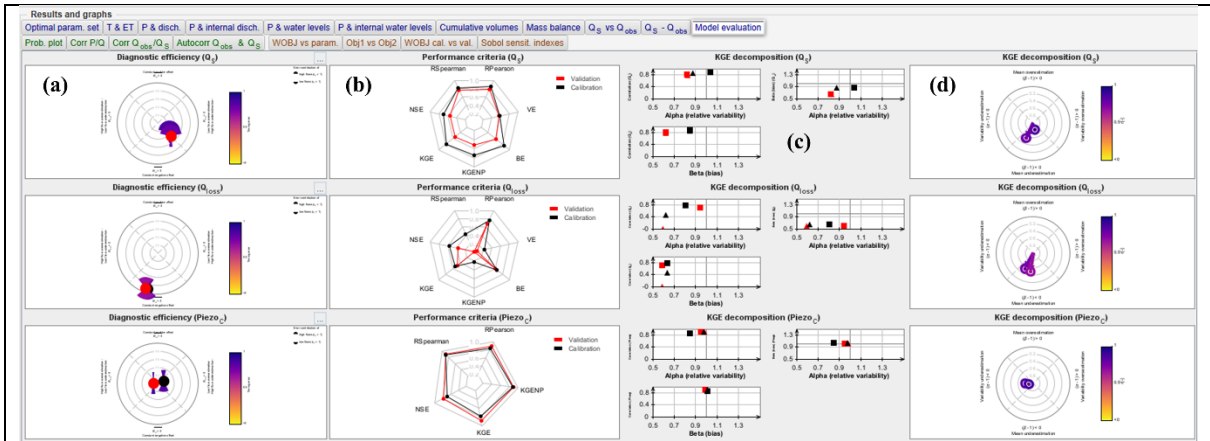


**Fig. 9 Screenshot of KarstMod with a focus on the sub-panel "Model evaluation". Application for the model evaluation on the Lez system. The panel is composed such as (i) each row corresponds to the variable for calibration ( $Q_s$ ,  $Q_{loss}$  and  $PiezoC$ ) and (ii) each column corresponds to (a) diagnostic efficiency plot, (b) radar plots, one should note that VE and BE are not computed according to the piezometric time series, (c) decomposition of KGE (square) and KGENP (triangle) and (d) radar plot of the KGE decomposition.**

447 **5 Conclusion**

448 KarstMod consists of a useful tool for the assessment of karst groundwater variability and sensitivity to  
 449 anthropogenic pressures (e.g., groundwater abstraction). This tool is devoted to promoting good  
 450 practices in hydrological modeling for learning and occasional users. KarstMod requires no  
 451 programming skills and offers a user-friendly interface allowing any user to easily manage hydrological  
 452 modeling. As a first step, KarstMod can be used to explore the ability of conceptual representations to  
 453 explain observations such as discharge or piezometric heads in karst systems. More advanced use of  
 454 KarstMod is also possible as it provides a complete framework for (i) primary analysis of the data, (ii)  
 455 comparison of various model structures, (iii) evaluation of the hydrological model performance as well  
 456 as (iv) first assessment of parametric uncertainties. The research community increasingly uses KarstMod  
 457 to address various challenges in karst hydrology, from understanding hydrological processes to practical  
 458 applications such as evaluation of groundwater management plans, or even assessment of the impact of  
 459 groundwater abstraction and climate changes on karst groundwater resources.

460 Future developments of KarstMod might include (i) the consideration of the spatial heterogeneity in  
 461 recharge processes which is essential when considering snowmelt as well as land cover (Sivelle et al.,  
 462 2022a), (ii) the simulation of electrical conductivity (Chang et al., 2021), major ions concentration  
 463 (Hartmann et al., 2013) or natural tracer such as air excess (Sivelle et al., 2022a), and (iii) the assessment  
 464 of structural uncertainty (Cousquer et al., 2022). KarstMod should tend toward an open source research  
 465 software to avoid duplication of efforts in karst hydrological modeling. Also, a Python version is  
 466 required for a better connection with an additional framework for sensitivity analysis such as SAFE  
 467 toolbox (Pianosi et al., 2015) and for model calibration procedures such as particle swarm optimization  
 468 (Eberhart and Kennedy, 1995; Lee, 2014). Finally, the development of the KarstMod modeling platform  
 469 will benefit better transparency and repeatability with an open-source approach, as observed on other  
 470 numerical tools (Pianosi et al., 2020).

471 Nomenclature.

<i>AET</i>	actual evapotranspiration (mm day <sup>-1</sup> )
<i>CFR</i>	refreezing coefficient (-)
<i>CWH</i>	liquid water holding capacity of snow (-)
<i>DE</i>	diagnostic efficiency DE (Schwemmler et al., 2021)
<i>ET</i>	evapotranspiration (mm day <sup>-1</sup> )
<i>KGE</i>	Kling-Gupta Efficiency (Gupta et al., 2009)
<i>KGENP</i>	non-parametric Kling-Gupta Efficiency (Pool et al., 2018)
<i>MF</i>	melt coefficient (mm °C <sup>-1</sup> day <sup>-1</sup> )
<i>P</i>	precipitation (mm day <sup>-1</sup> )
<i>P<sub>eff</sub></i>	effective precipitation (mm day <sup>-1</sup> )

$P_{sr}$	precipitation computed with the Snow Routine (mm day <sup>-1</sup> )
$P_{sr}^*$	precipitation for a single sub-catchment computed with the Snow Routine (mm day <sup>-1</sup> )
$PET$	potential evapotranspiration (mm day <sup>-1</sup> )
$R_p$	Pearson's correlation coefficient
$R_s$	Spearman rank correlation coefficient
NSE	Nash-Sutcliffe Efficiency (Nash and Sutcliffe, 1970)
$n_{obj}$	targeted number of parameter sets
$Q_A$	water discharge considered for the flow component A (m <sup>3</sup> s <sup>-1</sup> )
$T$	air temperature (°C)
$T_a$	active temperature for snowmelt (°C)
$T_n$	active temperature for refreezing (°C)
$t_{max}$	maximum duration for sampling the parameter space (seconds)
$T_s$	temperature threshold (°C)
$U$	observations considered for parameter estimation
VE	volumetric error (Criss and Winston, 2008)
$Z_A$	water level considered for element A (m a.sl.)
$\phi$	performance criteria
$\Phi$	objective function

472 Code availability. The KarstMod modeling platform is developed and made freely accessible within the  
473 framework of the KARST observatory network (SNO KARST) initiative from the INSU/CNRS. The  
474 platform can be downloaded here: <https://sokarst.org/en/software-en/karstmod-en/>

475 Author contributions. V. Sivelles: methodology, software, writing—original draft. G. Cinkus:  
476 methodology, software, writing—review, and editing. N. Mazzilli: methodology, software, project  
477 administration, writing—review and editing. H. Jourde: methodology, software, project administration,  
478 funding acquisition, writing—review and editing. D. Labat: methodology, software, writing—review,  
479 and editing. B. Arfib: methodology, software, writing—review and editing. N. Massei: methodology,  
480 software, writing—review and editing. Y. Cousquer: writing—review and editing. D. Bertin:  
481 methodology, software, writing—review, and editing.

482 Competing interests. The authors declare no competing interest.

483 Acknowledgements. This platform is developed within the framework of the KARST observatory  
484 network (SNO KARST) initiative from the INSU/CNRS (France), which aims to strengthen knowledge-  
485 sharing and promote crossdisciplinarity in research on karst systems at the national scale. This work, as  
486 well as V. Sivelles's post-doctoral position, was supported by the European Commission through the

487 Partnership for Research and Innovation in the Mediterranean Area (PRIMA) program under Horizon  
488 2020 (KARMA project, grant agreement number 01DH19022A).

489 **References**

- 490 Andréassian, V.: On the (im)possible validation of hydrogeological models, *Comptes Rendus.*  
491 *Géoscience*, 355, 1–9, <https://doi.org/10.5802/crgeos.142>, 2023.
- 492 Avias, J. V.: Gestion active de l'exurgence karstique de la Source du Lez (Hérault, France) 1957-1994,  
493 *Hydrogéologie (Orléans)*, 113–127, 1995.
- 494 Bailly-Comte, V., Martin, J. B., Jourde, H., Sreaton, E. J., Pistre, S., and Langston, A.: Water exchange  
495 and pressure transfer between conduits and matrix and their influence on hydrodynamics of two karst  
496 aquifers with sinking streams, *Journal of Hydrology*, 12, 2010.
- 497 Bennett, N. D., Croke, B. F. W., Guariso, G., Guillaume, J. H. A., Hamilton, S. H., Jakeman, A. J.,  
498 Marsili-Libelli, S., Newham, L. T. H., Norton, J. P., Perrin, C., Pierce, S. A., Robson, B., Seppelt, R.,  
499 Voinov, A. A., Fath, B. D., and Andreassian, V.: Characterising performance of environmental models,  
500 *Environmental Modelling & Software*, 40, 1–20, <https://doi.org/10.1016/j.envsoft.2012.09.011>, 2013.
- 501 Bérard, P.: Alimentation en eau de la ville de Montpellier: captage de la source du Lez—étude des  
502 relations entre la source et son réservoir aquifère [Water supply of Montpellier: Lez Spring catchment—  
503 study of the relationship between the spring and its aquifer], BRGM, Montpellier, France, 1983.
- 504 Bergström, S.: The HBV model - its structure and applications., 1992.
- 505 Beven, K.: On explanatory depth and predictive power, *Hydrological Processes*, 15, 3069–3072,  
506 <https://doi.org/10.1002/hyp.500>, 2001.
- 507 Beven, K.: A manifesto for the equifinality thesis, *Journal of Hydrology*, 320, 18–36,  
508 <https://doi.org/10.1016/j.jhydrol.2005.07.007>, 2006.
- 509 Bittner, D., Narany, T. S., Kohl, B., Disse, M., and Chiogna, G.: Modeling the hydrological impact of  
510 land use change in a dolomite-dominated karst system, *Journal of Hydrology*, 567, 267–279,  
511 <https://doi.org/10.1016/j.jhydrol.2018.10.017>, 2018.
- 512 Bittner, D., Richieri, B., and Chiogna, G.: Unraveling the time-dependent relevance of input model  
513 uncertainties for a lumped hydrologic model of a pre-alpine karst system, *Hydrogeol J*,  
514 <https://doi.org/10.1007/s10040-021-02377-1>, 2021.
- 515 Blöschl, G., Bierkens, M. F. P., Chambel, A., Cudennec, C., Destouni, G., Fiori, A., Kirchner, J. W.,  
516 McDonnell, J. J., Savenije, H. H. G., Sivapalan, M., Stumpp, C., Toth, E., Volpi, E., Carr, G., Lupton,  
517 C., Salinas, J., Széles, B., Viglione, A., Aksoy, H., Allen, S. T., Amin, A., Andréassian, V., Arheimer,  
518 B., Aryal, S. K., Baker, V., Bardsley, E., Barendrecht, M. H., Bartosova, A., Batelaan, O., Berghuijs,

519 W. R., Beven, K., Blume, T., Bogaard, T., Borges de Amorim, P., Böttcher, M. E., Boulet, G., Breinl,  
520 K., Brilly, M., Brocca, L., Buytaert, W., Castellarin, A., Castelletti, A., Chen, X., Chen, Y., Chen, Y.,  
521 Chiffard, P., Claps, P., Clark, M. P., Collins, A. L., Croke, B., Dathe, A., David, P. C., de Barros, F. P.  
522 J., de Rooij, G., Di Baldassarre, G., Driscoll, J. M., Duethmann, D., Dwivedi, R., Eris, E., Farmer, W.  
523 H., Feiccabrino, J., Ferguson, G., Ferrari, E., Ferraris, S., Fersch, B., Finger, D., Foglia, L., Fowler, K.,  
524 Gartsman, B., Gascoïn, S., Gaume, E., Gelfan, A., Geris, J., Gharari, S., Gleeson, T., Glendell, M.,  
525 Gonzalez Bevacqua, A., González-Dugo, M. P., Grimaldi, S., Gupta, A. B., Guse, B., Han, D., Hannah,  
526 D., Harpold, A., Haun, S., Heal, K., Helfricht, K., Herrnegger, M., Hipsey, M., Hlaváčiková, H.,  
527 Hohmann, C., Holko, L., Hopkinson, C., Hrachowitz, M., Illangasekare, T. H., Inam, A., Innocente, C.,  
528 Istanbuluoglu, E., Jarihani, B., et al.: Twenty-three unsolved problems in hydrology (UPH) – a  
529 community perspective, *Hydrological Sciences Journal*, 64, 1141–1158,  
530 <https://doi.org/10.1080/02626667.2019.1620507>, 2019.

531 Çallı, S. S., Çallı, K. Ö., Tuğrul Yılmaz, M., and Çelik, M.: Contribution of the satellite-data driven  
532 snow routine to a karst hydrological model, *Journal of Hydrology*, 607, 127511,  
533 <https://doi.org/10.1016/j.jhydrol.2022.127511>, 2022.

534 Chang, Y., Hartmann, A., Liu, L., Jiang, G., and Wu, J.: Identifying More Realistic Model Structures  
535 by Electrical Conductivity Observations of the Karst Spring, *Water Resources Research*, 57,  
536 e2020WR028587, <https://doi.org/10.1029/2020WR028587>, 2021.

537 Chen, Z. and Goldscheider, N.: Modeling spatially and temporally varied hydraulic behavior of a folded  
538 karst system with dominant conduit drainage at catchment scale, Hochifen–Gottesacker, Alps, *Journal*  
539 *of Hydrology*, 514, 41–52, <https://doi.org/10.1016/j.jhydrol.2014.04.005>, 2014.

540 Chen, Z., Hartmann, A., Wagener, T., and Goldscheider, N.: Dynamics of water fluxes and storages in  
541 an Alpine karst catchment under current and potential future climate conditions, *Hydrology and Earth*  
542 *System Sciences*, 22, 3807–3823, <https://doi.org/10.5194/hess-22-3807-2018>, 2018.

543 Cinkus, G., Wunsch, A., Mazzilli, N., Liesch, T., Chen, Z., Ravbar, N., Doummar, J., Fernández-Ortega,  
544 J., Barberá, J. A., Andreo, B., Goldscheider, N., and Jourde, H.: Comparison of artificial neural networks  
545 and reservoir models for simulating karst spring discharge on five test sites in the Alpine and  
546 Mediterranean regions, *Hydrology and Earth System Sciences*, 27, 1961–1985,  
547 <https://doi.org/10.5194/hess-27-1961-2023>, 2023a.

548 Cinkus, G., Mazzilli, N., Jourde, H., Wunsch, A., Liesch, T., Ravbar, N., Chen, Z., and Goldscheider,  
549 N.: When best is the enemy of good – critical evaluation of performance criteria in hydrological models,  
550 *Hydrology and Earth System Sciences*, 27, 2397–2411, <https://doi.org/10.5194/hess-27-2397-2023>,  
551 2023b.

552 Clauzon, V., Mayolle, S., Leonardi, V., Brunet, P., Soliva, R., Marchand, P., Massonnat, G., Rolando,  
553 J.-P., and Pistre, S.: Fault zones in limestones: impact on karstogenesis and groundwater flow (Lez  
554 aquifer, southern France), *Hydrogeol J*, <https://doi.org/10.1007/s10040-020-02189-9>, 2020.

555 Cos, J., Doblas-Reyes, F., Jury, M., Marcos, R., Bretonnière, P.-A., and Samsó, M.: The Mediterranean  
556 climate change hotspot in the CMIP5 and CMIP6 projections, *Earth System Dynamics*, 13, 321–340,  
557 <https://doi.org/10.5194/esd-13-321-2022>, 2022.

558 Cousquer, Y. and Jourde, H.: Reducing Uncertainty of Karst Aquifer Modeling with Complementary  
559 Hydrological Observations for the Sustainable Management of Groundwater Resources, *Journal of*  
560 *Hydrology*, 128130, <https://doi.org/10.1016/j.jhydrol.2022.128130>, 2022.

561 Cousquer, Y., Sivelles, V., and Jourde, H.: Estimating the Structural Uncertainty of Lumped Parameter  
562 Models in Karst Hydrology: a Bayesian Model Averaging (BMA), *Copernicus Meetings*, 2022.

563 Criss, R. E. and Winston, W. E.: Do Nash values have value? Discussion and alternate proposals,  
564 *Hydrological Processes*, 22, 2723–2725, <https://doi.org/10.1002/hyp.7072>, 2008.

565 Dakhlaoui, H. and Djebbi, K.: Evaluating the impact of rainfall–runoff model structural uncertainty on  
566 the hydrological rating of regional climate model simulations, *Journal of Water and Climate Change*,  
567 12, 3820–3838, <https://doi.org/10.2166/wcc.2021.004>, 2021.

568 Darbandsari, P. and Coulibaly, P.: Inter-comparison of lumped hydrological models in data-scarce  
569 watersheds using different precipitation forcing data sets: Case study of Northern Ontario, Canada,  
570 *Journal of Hydrology: Regional Studies*, 31, 100730, <https://doi.org/10.1016/j.ejrh.2020.100730>, 2020.

571 Diffenbaugh, N. S. and Giorgi, F.: Climate change hotspots in the CMIP5 global climate model  
572 ensemble, *Climatic Change*, 114, 813–822, <https://doi.org/10.1007/s10584-012-0570-x>, 2012.

573 Doummar, J., Sauter, M., and Geyer, T.: Simulation of flow processes in a large scale karst system with  
574 an integrated catchment model (Mike She) – Identification of relevant parameters influencing spring  
575 discharge, *Journal of Hydrology*, 426–427, 112–123, <https://doi.org/10.1016/j.jhydrol.2012.01.021>,  
576 2012.

577 Doummar, J., Hassan Kassem, A., and Gurdak, J. J.: Impact of historic and future climate on spring  
578 recharge and discharge based on an integrated numerical modelling approach: Application on a snow-  
579 governed semi-arid karst catchment area, *Journal of Hydrology*, 565, 636–649,  
580 <https://doi.org/10.1016/j.jhydrol.2018.08.062>, 2018.



581 Dubois, E., Doummar, J., Pistre, S., and Larocque, M.: Calibration of a lumped karst system model and  
582 application to the Qachqouch karst spring (Lebanon) under climate change conditions, *Hydrology and*  
583 *Earth System Sciences*, 24, 4275–4290, <https://doi.org/10.5194/hess-24-4275-2020>, 2020.

584 Duran, L., Massei, N., Lecoq, N., Fournier, M., and Labat, D.: Analyzing multi-scale hydrodynamic  
585 processes in karst with a coupled conceptual modeling and signal decomposition approach, *Journal of*  
586 *Hydrology*, 583, 124625, <https://doi.org/10.1016/j.jhydrol.2020.124625>, 2020.

587 Ebel, B. A. and Loague, K.: Physics-based hydrologic-response simulation: Seeing through the fog of  
588 equifinality, *Hydrological Processes*, 20, 2887–2900, <https://doi.org/10.1002/hyp.6388>, 2006.

589 Eberhart, R. and Kennedy, J.: Particle swarm optimization, in: *Proceedings of the IEEE international*  
590 *conference on neural networks*, 1942–1948, 1995.

591 Elshall, A. S., Arik, A. D., El-Kadi, A. I., Pierce, S., Ye, M., Burnett, K. M., Wada, C. A., Bremer, L.  
592 L., and Chun, G.: Groundwater sustainability: a review of the interactions between science and policy,  
593 *Environ. Res. Lett.*, 15, 093004, <https://doi.org/10.1088/1748-9326/ab8e8c>, 2020.

594 Ferreira, P. M. de L., Paz, A. R. da, and Bravo, J. M.: Objective functions used as performance metrics  
595 for hydrological models: state-of-the-art and critical analysis, *RBRH*, 25, e42,  
596 <https://doi.org/10.1590/2318-0331.252020190155>, 2020.

597 Ficchi, A., Perrin, C., and Andréassian, V.: Impact of temporal resolution of inputs on hydrological  
598 model performance: An analysis based on 2400 flood events, *Journal of Hydrology*, 538, 454–470,  
599 <https://doi.org/10.1016/j.jhydrol.2016.04.016>, 2016.

600 Fiorillo, F., Leone, G., Pagnozzi, M., and Esposito, L.: Long-term trends in karst spring discharge and  
601 relation to climate factors and changes, *Hydrogeol J*, 29, 347–377, [https://doi.org/10.1007/s10040-020-](https://doi.org/10.1007/s10040-020-02265-0)  
602 [02265-0](https://doi.org/10.1007/s10040-020-02265-0), 2021.

603 Fleury, P., Plagnes, V., and Bakalowicz, M.: Modelling of the functioning of karst aquifers with a  
604 reservoir model: Application to Fontaine de Vaucluse (South of France), *Journal of Hydrology*, 345,  
605 38–49, <https://doi.org/10.1016/j.jhydrol.2007.07.014>, 2007.

606 Fleury, P., Ladouche, B., Conroux, Y., Jourde, H., and Dörfliger, N.: Modelling the hydrologic functions  
607 of a karst aquifer under active water management – The Lez spring, *Journal of Hydrology*, 365, 235–  
608 243, <https://doi.org/10.1016/j.jhydrol.2008.11.037>, 2009.

609 Ford, D. and Williams, P.: *Karst hydrogeology and geomorphology*, John Wiley & Sons, Hoboken, NJ,  
610 USA, 2013.

611 Frank, S., Goeppert, N., and Goldscheider, N.: Improved understanding of dynamic water and mass  
612 budgets of high-alpine karst systems obtained from studying a well-defined catchment area,  
613 *Hydrological Processes*, 35, e14033, <https://doi.org/10.1002/hyp.14033>, 2021.

614 Freedman, D., Pisani, R., Purves, R., and Adhikari, A.: *Statistics*, WW Norton & Company New York,  
615 2007.

616 Guinot, V., Savéan, M., Jourde, H., and Neppel, L.: Conceptual rainfall–runoff model with a two-  
617 parameter, infinite characteristic time transfer function, *Hydrological Processes*, 29, 4756–4778,  
618 <https://doi.org/10.1002/hyp.10523>, 2015.

619 Gupta, A. and Govindaraju, R. S.: Propagation of structural uncertainty in watershed hydrologic models,  
620 *Journal of Hydrology*, 575, 66–81, <https://doi.org/10.1016/j.jhydrol.2019.05.026>, 2019.

621 Gupta, H. V., Kling, H., Yilmaz, K. K., and Martinez, G. F.: Decomposition of the mean squared error  
622 and NSE performance criteria: Implications for improving hydrological modelling, *Journal of*  
623 *Hydrology*, 377, 80–91, <https://doi.org/10.1016/j.jhydrol.2009.08.003>, 2009.

624 Hartmann, A., Lange, J., Vivó Aguado, À., Mizyed, N., Smiatek, G., and Kunstmann, H.: A multi-model  
625 approach for improved simulations of future water availability at a large Eastern Mediterranean karst  
626 spring, *Journal of Hydrology*, 468–469, 130–138, <https://doi.org/10.1016/j.jhydrol.2012.08.024>, 2012.

627 Hartmann, A., Wagener, T., Rimmer, A., Lange, J., Brielmann, H., and Weiler, M.: Testing the realism  
628 of model structures to identify karst system processes using water quality and quantity signatures, *Water*  
629 *Resour. Res.*, 49, 3345–3358, <https://doi.org/10.1002/wrcr.20229>, 2013.

630 Hauduc, H., Neumann, M. B., Muschalla, D., Gamerith, V., Gillot, S., and Vanrolleghem, P. A.:  
631 Efficiency criteria for environmental model quality assessment: A review and its application to  
632 wastewater treatment, *Environmental Modelling & Software*, 68, 196–204,  
633 <https://doi.org/10.1016/j.envsoft.2015.02.004>, 2015.

634 Jackson, E. K., Roberts, W., Nelsen, B., Williams, G. P., Nelson, E. J., and Ames, D. P.: Introductory  
635 overview: Error metrics for hydrologic modelling – A review of common practices and an open source  
636 library to facilitate use and adoption, *Environmental Modelling & Software*, 119, 32–48,  
637 <https://doi.org/10.1016/j.envsoft.2019.05.001>, 2019.

638 Jeannin, P.-Y., Artigue, G., Butscher, C., Chang, Y., Charlier, J.-B., Duran, L., Gill, L., Hartmann, A.,  
639 Johannet, A., Jourde, H., Kavousi, A., Liesch, T., Liu, Y., Lüthi, M., Malard, A., Mazzilli, N., Pardo-  
640 Igúzquiza, E., Thiéry, D., Reimann, T., Schuler, P., Wöhling, T., and Wunsch, A.: Karst modelling

641 challenge 1: Results of hydrological modelling, *Journal of Hydrology*, 126508,  
642 <https://doi.org/10.1016/j.jhydrol.2021.126508>, 2021.

643 Jiang, T., Chen, Y. D., Xu, C., Chen, X., Chen, X., and Singh, V. P.: Comparison of hydrological impacts  
644 of climate change simulated by six hydrological models in the Dongjiang Basin, South China, *Journal*  
645 *of Hydrology*, 336, 316–333, <https://doi.org/10.1016/j.jhydrol.2007.01.010>, 2007.

646 Jones, R. N., Chiew, F. H. S., Boughton, W. C., and Zhang, L.: Estimating the sensitivity of mean annual  
647 runoff to climate change using selected hydrological models, *Advances in Water Resources*, 29, 1419–  
648 1429, <https://doi.org/10.1016/j.advwatres.2005.11.001>, 2006.

649 Jourde, H., Lafare, A., Mazzilli, N., Belaud, G., Neppel, L., Dörfli, N., and Cernesson, F.: Flash flood  
650 mitigation as a positive consequence of anthropogenic forcing on the groundwater resource in a karst  
651 catchment, *Environ Earth Sci*, 71, 573–583, <https://doi.org/10.1007/s12665-013-2678-3>, 2014.

652 Klemeš, V.: Operational testing of hydrological simulation models, *Hydrological Sciences Journal*, 31,  
653 13–24, <https://doi.org/10.1080/02626668609491024>, 1986.

654 Knoben, W. J. M., Freer, J. E., Peel, M. C., Fowler, K. J. A., and Woods, R. A.: A Brief Analysis of  
655 Conceptual Model Structure Uncertainty Using 36 Models and 559 Catchments, *Water Resources*  
656 *Research*, 56, e2019WR025975, <https://doi.org/10.1029/2019WR025975>, 2020.

657 Labat, D., Argouze, R., Mazzilli, N., Ollivier, C., and Sivel, V.: Impact of Withdrawals on Karst  
658 Watershed Water Supply, *Water*, 14, 1339, <https://doi.org/10.3390/w14091339>, 2022.

659 Lee, A.: pyswarm: Particle swarm optimization (PSO) with constraint support, 2014.

660 Liu, Y., Wagener, T., and Hartmann, A.: Assessing Streamflow Sensitivity to Precipitation Variability  
661 in Karst-Influenced Catchments With Unclosed Water Balances, *Water Resources Research*, 57,  
662 e2020WR028598, <https://doi.org/10.1029/2020WR028598>, 2021.

663 Mazzilli, N. and Bertin, D.: *KarstMod User Guide - version 2.2*, 2019.

664 Mazzilli, N., Guinot, V., and Jourde, H.: Sensitivity analysis of conceptual model calibration to  
665 initialisation bias. Application to karst spring discharge models, *Advances in Water Resources*, 42, 1–  
666 16, <https://doi.org/10.1016/j.advwatres.2012.03.020>, 2012.

667 Mazzilli, N., Guinot, V., Jourde, H., Lecoq, N., Labat, D., Arfib, B., Baudement, C., Danquigny, C., Dal  
668 Soglio, L., and Bertin, D.: *KarstMod: A modelling platform for rainfall - discharge analysis and*  
669 *modelling dedicated to karst systems*, *Environmental Modelling & Software*, 122, 103927,  
670 <https://doi.org/10.1016/j.envsoft.2017.03.015>, 2019.

671 Mazzilli, N., Sivelles, V., Cinkus, G., Jourde, H., and Bertin, D.: KarstMod User Guide - version 3.0,  
672 2022.

673 McMillan, H., Jackson, B., Clark, M., Kavetski, D., and Woods, R.: Rainfall uncertainty in hydrological  
674 modelling: An evaluation of multiplicative error models, *Journal of Hydrology*, 400, 83–94,  
675 <https://doi.org/10.1016/j.jhydrol.2011.01.026>, 2011.

676 Moges, E., Demissie, Y., Larsen, L., and Yassin, F.: Review: Sources of Hydrological Model  
677 Uncertainties and Advances in Their Analysis, *Water*, 13, 28, <https://doi.org/10.3390/w13010028>, 2021.

678 Moriasi, D. N., Arnold, J. G., Liew, M. W. V., Bingner, R. L., Harmel, R. D., and Veith, T. L.: Model  
679 Evaluation Guidelines for Systematic Quantification of Accuracy in Watershed Simulations,  
680 *Transactions of the ASABE*, 50, 885–900, <https://doi.org/10.13031/2013.23153>, 2007.

681 Nash, J. E. and Sutcliffe, J. V.: River flow forecasting through conceptual models part I — A discussion  
682 of principles, *Journal of Hydrology*, 10, 282–290, [https://doi.org/10.1016/0022-1694\(70\)90255-6](https://doi.org/10.1016/0022-1694(70)90255-6), 1970.

683 Nerantzaki, S. D. and Nikolaidis, N. P.: The response of three Mediterranean karst springs to drought  
684 and the impact of climate change, *Journal of Hydrology*, 591, 125296,  
685 <https://doi.org/10.1016/j.jhydrol.2020.125296>, 2020.

686 Ollivier, C., Mazzilli, N., Oliosio, A., Chalikakis, K., Carrière, S. D., Danquigny, C., and Emblanch, C.:  
687 Karst recharge-discharge semi distributed model to assess spatial variability of flows, *Science of The*  
688 *Total Environment*, 703, 134368, <https://doi.org/10.1016/j.scitotenv.2019.134368>, 2020.

689 Oudin, L., Hervieu, F., Michel, C., Perrin, C., Andréassian, V., Anctil, F., and Loumagne, C.: Which  
690 potential evapotranspiration input for a lumped rainfall–runoff model? Part 2—Towards a simple and  
691 efficient potential evapotranspiration model for rainfall–runoff modelling, *Journal of Hydrology*, 303,  
692 290–306, <https://doi.org/10.1016/j.jhydrol.2004.08.026>, 2005.

693 Pandi, D., Kothandaraman, S., and Kuppasamy, M.: Hydrological models: a review, *International*  
694 *Journal of Hydrology Science and Technology*, 12, 223–242,  
695 <https://doi.org/10.1504/IJHST.2021.117540>, 2021.

696 Pechlivanidis, I., Jackson, B., McMillan, H., and Gupta, H. V.: Using an informational entropy-based  
697 metric as a diagnostic of flow duration to drive model parameter identification, *Global NEST Journal*,  
698 14, 325–334, <https://doi.org/10.30955/gnj.000879>, 2013.

699 Perrin, C., Michel, C., and Andréassian, V.: Does a large number of parameters enhance model  
700 performance? Comparative assessment of common catchment model structures on 429 catchments,  
701 *Journal of Hydrology*, 242, 275–301, [https://doi.org/10.1016/S0022-1694\(00\)00393-0](https://doi.org/10.1016/S0022-1694(00)00393-0), 2001.

702 Pianosi, F., Sarrazin, F., and Wagener, T.: A Matlab toolbox for Global Sensitivity Analysis,  
703 *Environmental Modelling & Software*, 70, 80–85, <https://doi.org/10.1016/j.envsoft.2015.04.009>, 2015.

704 Pianosi, F., Sarrazin, F., and Wagener, T.: How successfully is open-source research software adopted?  
705 Results and implications of surveying the users of a sensitivity analysis toolbox, *Environmental*  
706 *Modelling & Software*, 124, 104579, <https://doi.org/10.1016/j.envsoft.2019.104579>, 2020.

707 Pool, S., Vis, M., and Seibert, J.: Evaluating model performance: towards a non-parametric variant of  
708 the Kling-Gupta efficiency, *Hydrological Sciences Journal*, 63, 1941–1953,  
709 <https://doi.org/10.1080/02626667.2018.1552002>, 2018.

710 Poulain, A., Watlet, A., Kaufmann, O., Van Camp, M., Jourde, H., Mazzilli, N., Rochez, G., Deleu, R.,  
711 Quinif, Y., and Hallet, V.: Assessment of groundwater recharge processes through karst vadose zone by  
712 cave percolation monitoring, *Hydrological Processes*, 32, 2069–2083,  
713 <https://doi.org/10.1002/hyp.13138>, 2018.

714 Sarrazin, F., Hartmann, A., Pianosi, F., Rosolem, R., and Wagener, T.: V2Karst V1.1: a parsimonious  
715 large-scale integrated vegetation–recharge model to simulate the impact of climate and land cover  
716 change in karst regions, *Geosci. Model Dev.*, 11, 4933–4964, [https://doi.org/10.5194/gmd-11-4933-](https://doi.org/10.5194/gmd-11-4933-2018)  
717 2018, 2018.

718 Schwemmler, R., Demand, D., and Weiler, M.: Technical note: Diagnostic efficiency – specific  
719 evaluation of model performance, *Hydrology and Earth System Sciences*, 25, 2187–2198,  
720 <https://doi.org/10.5194/hess-25-2187-2021>, 2021.

721 Shmueli, G.: To Explain or to Predict?, *Statistical Science*, 25, 289–310, [https://doi.org/10.1214/10-](https://doi.org/10.1214/10-STS330)  
722 STS330, 2010.

723 Sivellev, V. and Jourde, H.: A methodology for the assessment of groundwater resource variability in  
724 karst catchments with sparse temporal measurements, *Hydrogeol J*, 29, 137–157,  
725 <https://doi.org/10.1007/s10040-020-02239-2>, 2020.

726 Sivellev, V., Labat, D., Mazzilli, N., Massei, N., and Jourde, H.: Dynamics of the Flow Exchanges  
727 between Matrix and Conduits in Karstified Watersheds at Multiple Temporal Scales, *Water*, 11, 569,  
728 <https://doi.org/10.3390/w11030569>, 2019.

729 Sivellev, V., Jourde, H., Bittner, D., Mazzilli, N., and Trambalay, Y.: Assessment of the relative impacts  
730 of climate changes and anthropogenic forcing on spring discharge of a Mediterranean karst system,  
731 *Journal of Hydrology*, 598, 126396, <https://doi.org/10.1016/j.jhydrol.2021.126396>, 2021.

732 Sivellev, V., Pérotin, L., Ladouche, B., de Montety, V., Bailly-Comte, V., Champollion, C., and Jourde,  
733 H.: A lumped parameter model to evaluate the relevance of excess air as a tracer of exchanged flows  
734 between transmissive and capacitive compartments of karst systems, *Frontiers in Water*, 4, 2022a.

735 Sivellev, V., Jourde, H., Bittner, D., Richieri, B., Labat, D., Hartmann, A., and Chiogna, G.: Considering  
736 land cover and land use (LCLU) in lumped parameter modeling in forest dominated karst catchments,  
737 *Journal of Hydrology*, 612, 128264, <https://doi.org/10.1016/j.jhydrol.2022.128264>, 2022b.

738 Smiatek, G., Kaspar, S., and Kunstmann, H.: Hydrological Climate Change Impact Analysis for the  
739 Figeih Spring near Damascus, Syria, *Journal of Hydrometeorology*, 14, 577–593,  
740 <https://doi.org/10.1175/JHM-D-12-065.1>, 2013.

741 Sobol, I. M.: On quasi-Monte Carlo integrations, *Mathematics and Computers in Simulation*, 47, 103–  
742 112, [https://doi.org/10.1016/S0378-4754\(98\)00096-2](https://doi.org/10.1016/S0378-4754(98)00096-2), 1998.

743 Sophocleous, M.: Interactions between groundwater and surface water: the state of the science,  
744 *Hydrogeology Journal*, 10, 52–67, <https://doi.org/10.1007/s10040-001-0170-8>, 2002.

745 Stevanović, Z.: Karst waters in potable water supply: a global scale overview, *Environ Earth Sci*, 78,  
746 662, <https://doi.org/10.1007/s12665-019-8670-9>, 2019.

747 Westerberg, I. K., Sikorska-Senoner, A. E., Viviroli, D., Vis, M., and Seibert, J.: Hydrological model  
748 calibration with uncertain discharge data, *Hydrological Sciences Journal*, 0, null,  
749 <https://doi.org/10.1080/02626667.2020.1735638>, 2020.

750 Zhou, S., Wang, Y., Li, Z., Chang, J., and Guo, A.: Quantifying the Uncertainty Interaction Between  
751 the Model Input and Structure on Hydrological Processes, *Water Resour Manage*, 35, 3915–3935,  
752 <https://doi.org/10.1007/s11269-021-02883-7>, 2021.

753